PHYSICAL REVIEW C **84**, 054614 (2011)

Cluster transfer in the reaction $^{16}O + ^{208}Pb$ at energies well below the fusion barrier: A possible doorway to energy dissipation

M. Evers,* M. Dasgupta, D. J. Hinde, D. H. Luong, R. Rafiei,† and R. du Rietz
Department of Nuclear Physics, Research School of Physics and Engineering, Australian National University, Canberra, Australian Capital Territory 0200, Australia

C. Simenel‡
CEA, Centre de Saclay, IRFU/Service de Physique Nucléaire, F-91191 Gif-sur-Yvette, France
(Received 30 September 2011; published 22 November 2011)

The reaction $^{16}O + ^{208}Pb$ is a benchmark in nuclear reaction studies as it involves two doubly magic nuclei. New measurements of back-scattered projectile-like fragments at sub-barrier energies show that the probability of two-proton ($2p$) transfer is much larger than that of α-particle transfer. At energies around the fusion barrier the probability for $2p$ transfer is $\sim$10%, similar to that for one-proton transfer. The $2p$ transfer probabilities are enhanced by up to an order of magnitude compared to calculations based on an independent particle picture as simulated by the fully microscopic time-dependent Hartree-Fock model (TDHF). Since beyond mean-field correlations like nucleon pairing are not included in the TDHF model, the enhancement indicates strong pairing correlations between the transferred protons. $2p$ transfer leads to excitation energies (most likely in the target-like nucleus) up to $\sim$13 MeV, indicating that it may represent an effective doorway for the dissipation of energy and thus provide a microscopic mechanism toward understanding the inhibition of fusion and energies both above and below the barrier.

DOI: 10.1103/PhysRevC.84.054614 PACS number(s): 25.70.Hi, 21.60.Gx

I. INTRODUCTION

Collisions of heavy ions at energies well below and close to the fusion barrier are entirely driven by quantum mechanics. For example, sub-barrier fusion occurs through quantum tunneling of the projectile nucleus through the fusion barrier. This process in turn is affected by the internal structure of the collision partners [1]. Coupled reaction channels calculations that consider colliding nuclei to be in a coherent superposition of their intrinsic states are very successful in describing fusion at energies around the fusion barrier. However, at deep sub-barrier energies, measured fusion probabilities are often significantly lower than those predicted by coupled reaction channels calculations using standard Woods-Saxon potentials [2–5]. This suppression of tunneling at deep sub-barrier energies has been observed in a range of different reactions and has been the source of ongoing discussions, triggering a renewed interest in understanding the details of reaction mechanisms at sub-barrier energies [6–9]. At above-barrier energies fusion cross sections also lie significantly below standard coupled-channels calculations [4,10]. This above-barrier fusion suppression was analyzed for different reactions [10] and was found to increase with the charge product of the colliding nuclei.

Quasi-elastic scattering, generally understood to include inelastic scattering and few-nucleon transfer to low-lying states in the residual nuclei, has proven to be a useful tool to investigate the interplay of different processes at sub-barrier energies (see, e.g., [11–17]). Measurements of the individual projectile-like fragment (PLF) yields provide insight into the different underlying peripheral reaction processes. Among the possible quasi-elastic reaction processes that can affect fusion, transfer of more than one nucleon is certainly the least well understood process and constitutes an important task to be described both experimentally and theoretically.

The distinction between sequential and cluster transfer is a great challenge, not only in nuclear physics [18] but also in electron transfer between ions or atomic cluster collisions [19]. In nuclear collisions, the transfer of a cluster of nucleons is a clear signature of correlations between the transferred nucleons affecting the dynamics. Pairing between nucleons of the same isospin (i.e., proton-proton and neutron-neutron pairing) as well as α-particle clustering have been considered as the most important correlations affecting multinucleon transfer [18]. Measurements of transfer probabilities in various reactions at energies near the fusion barrier have therefore been utilized to investigate the role of pairing correlations between the transferred nucleons. Pairing correlations are believed to lead to a significant enhancement of pair and multipair transfer probabilities [18,20–24]. Frequently related to the phenomenon of pairing correlations is the nuclear Josephson effect [25], which is understood as the tunneling of nucleon pairs (i.e., nuclear Cooper pairs) through a time-dependent barrier at energies near but below the fusion barrier. This effect is believed to be similar to that of a supercurrent between two superconductors separated by an insulator. An enhancement of

*maurits.evers@anu.edu.au
†Current address: Australian Nuclear Science and Technology Organisation (ANSTO), Lucas Heights, NSW 2232, Australia.
‡Current address: Department of Nuclear Physics, Research School of Physics and Engineering, Australian National University, Canberra, Australian Capital Territory 0200, Australia.

the transfer probability at sub-barrier energies may therefore be related to the tunneling of Cooper pairs from one superfluid nucleus to the other [18].

With respect to the effect of transfer on fusion, there is as yet no understanding of a mechanism by which multinucleon transfer to low-lying states could suppress fusion, either below or above the barrier. However, it has been argued [10,26] that the suppression of fusion above the barrier can be associated with deep inelastic collisions (DICs), which can result in highly excited projectile-like and/or target-like nuclei through the dissipation of kinetic energy into the internal nucleonic degrees of freedom of the residual nuclei, already at nuclear separations outside the fusion barrier. Measurements of these DIC products [23,27] show that both energy dissipation and nucleon transfer are important and related to each other. We expect in reality a smooth transition from nucleon transfer to low-lying discrete states in quasi-elastic scattering on one end to (multi)nucleon transfer leading to energy dissipation in DICs at energies above the barrier on the other end. From a classical (or semiclassical) point of view, the dissipation of energy will result in some trajectories failing to overcome the fusion barrier and thus to a suppression of fusion. However, it is not clear whether the concept of energy dissipation is significant in reactions involving lighter nuclei, such as ^{16}O + ^{208}Pb. It is thus uncertain which mechanism(s) might be responsible for the observed suppression of fusion in this reaction [4].

The reaction ^{16}O + ^{208}Pb can be considered a benchmark in low-energy heavy-ion collisions [28–35]. In the independent particle shell model, both nuclei are doubly magic with a closed shell of protons and neutrons. Both nuclei have a large energy gap to the next unoccupied shell. Hence it might be expected that the occupancy of states below the Fermi surface should be essentially unity. However, one- and two-proton knockout measurements on ^{16}O through inelastic electron scattering show a reduction of the spectroscopic factors of single-particle states in ^{16}O just below the Fermi surface [36–38]. This indicates that nucleon correlations play an important role even in the structure of ^{16}O. Indeed, ^{16}O is a good candidate for α clustering, and α condensates have been predicted [39] and successfully studied experimentally [40,41].

The measurement of transfer reactions themselves is a natural approach to investigate such correlations. Measurements probing different transfer channels for the ^{16}O + ^{208}Pb reaction exist [34,42], however mostly at energies near and well above the fusion barrier. It was commonly expected that the dominant transfer process involving the exchange of two charged nucleons at energies *near the fusion barrier* should be α-particle transfer, through the stripping reaction ^{208}Pb(^{16}O,^{12}C)^{212}Po [28]– [30]. This expectation was based on the large α-particle binding energy [28]– [31] and is supported by the observed α condensation in ^{16}O. Although two-proton ($2p$) transfer in the stripping reaction ^{208}Pb(^{16}O,^{14}C)^{210}Po was measured at energies *well above the fusion barrier* [32–34], relative probabilities for α-particle and $2p$ transfer were not obtained. The difficulties commonly associated with the description of charged nucleon transfer [11,43] have led $2p$ and α-particle transfer to remain an enigma in nuclear collision studies over the past decades, and no global predictive model exists to our knowledge.

This paper presents evidence that (i) $\Delta Z = 2$ transfer probabilities are large in the reaction ^{16}O + ^{208}Pb at energies below and near the fusion barrier [$\sim$10% at beam energies near the fusion barrier, similar to those for one-proton ($1p$) transfer], (ii) $2p$ stripping (and not α-particle transfer) is the dominant $\Delta Z = 2$ transfer process at these energies, (iii) the probabilities for $2p$ transfer are significantly enhanced compared to calculations based on the time-dependent Hartree-Fock (TDHF) theory for the transfer of uncorrelated protons, and (iv) $2p$ transfer leads to excitation energies (most likely in the target-like nucleus) as high as $\sim$13 MeV at beam energies near, but still below, the fusion barrier. Results in this paper show that experimental and theoretical work on multinucleon transfer, particularly cluster transfer, in heavy-ion collisions may be a key toward developing a complete understanding of both fusion and reflected flux in low-energy heavy-ion collisions.

II. MEASUREMENTS AND ANALYSIS

Measurements were carried out using the 14UD electrostatic accelerator of the Heavy-Ion Accelerator Facility at the Australian National University. Beams of ^{16}O were incident on a ^{208}PbS target with a thickness of 100 μg/cm^2, evaporated onto a 15 μg/cm^2 C backing, facing downstream. Two Si detectors (monitors) positioned at $\pm 30^\circ$ were used to normalize the back-scattered events to the Rutherford cross section. Using a Si detector located at a backward angle of $\theta_{\rm lab} = 162^\circ$ the energy $E_{\rm Si}$ of the back-scattered PLFs was recorded (energy FWHM $\sim$0.6 MeV). A typical energy spectrum for a measurement at a beam energy corresponding to $E_{\rm c.m.}/V_B = 0.98$ is shown in the top panel of Fig. 1, where $V_B = 74.5$ MeV is the experimental average fusion barrier energy [44]. Events are shown as a function of the total kinetic energy loss (TKEL), where the peak at TKEL = 0 corresponds to elastically scattered ^{16}O particles.

To resolve the different peripheral reaction processes and minimize background events, subsequent measurements recorded the PLFs using a detector telescope consisting of a propane-gas-filled ionization chamber and a Si detector, located at the same backward angle. Using this setup the energy $E_{\rm Si}$ and energy loss $\Delta E_{\rm gas}$ of the PLFs were recorded. A typical two-dimensional spectrum at a beam energy corresponding to $E_{\rm c.m.}/V_B = 0.98$ is shown in the top panel of Fig. 2. The three distinct regions correspond to oxygen, nitrogen, and carbon PLFs, which are associated with the transfer of $\Delta Z = 0, 1$, and 2 units of charge. The main peak at $E_{\rm Si} \sim 50$ MeV corresponds to elastically scattered ^{16}O particles. Events resulting from the transfer of three or more charged nucleons ($\Delta Z \geqslant 3$) were not observed at sub-barrier energies.

A. Isotopic identification of $\Delta Z = 2$ PLFs

In order to understand the $\Delta Z = 2$ transfer mechanisms, an identification of the dominant $\Delta Z = 2$ transfer process is important. Reaction Q values for $2p$ and α-particle stripping are too similar to allow separation of these processes solely based on kinematic considerations, as could be done for the $1p$

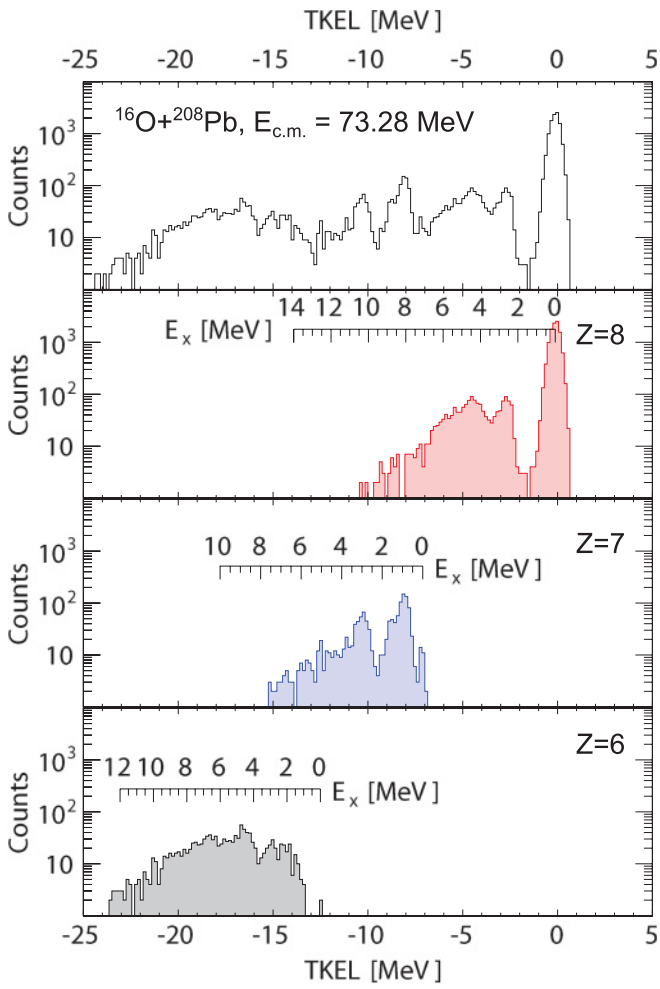

FIG. 1. (Color online) Energy spectra of the PLFs recorded at $\theta_{lab} = 162^\circ$, following the reaction $^{16}O + ^{208}Pb$ at the indicated beam energy, corresponding to $E_{c.m.}/V_B = 0.98$. The top panel shows the sum of all events as a function of the total kinetic energy loss (TKEL) assuming elastically scattered ^{16}O. The bottom three panels show the individual contributions of oxygen ($Z = 8$), nitrogen ($Z = 7$), and carbon ($Z = 6$) PLFs to the total E_{Si} spectrum. Separation of these events was achieved using a $\Delta E-E$ detector telescope (see text). In the bottom three panels, TKEL values have been converted to excitation energies E_x, assuming elastic scattering (for $Z = 8$), $1p$ stripping (for $Z = 7$), and $2p$ stripping (for $Z = 6$).

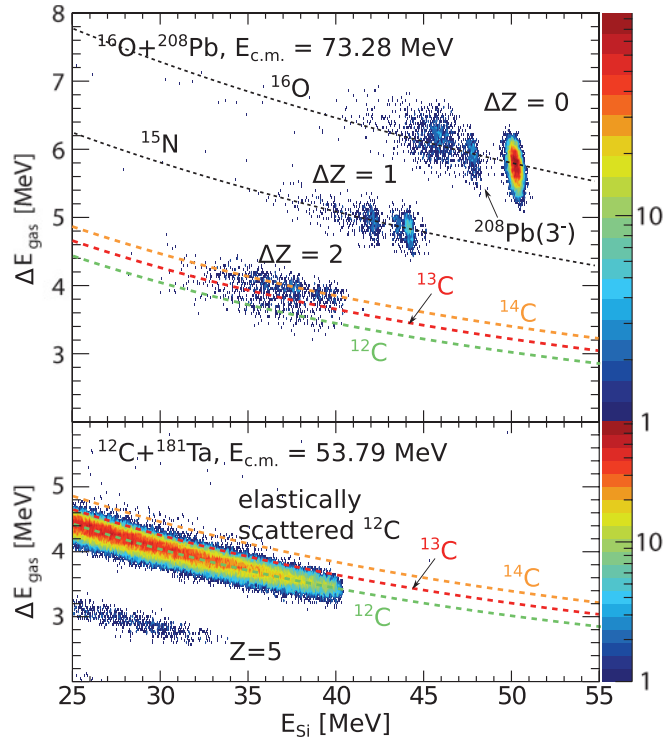

FIG. 2. (Color online) Top panel: Two-dimensional $\Delta E_{gas}-E_{Si}$ spectrum for the reaction $^{16}O + ^{208}Pb$ at the indicated beam energy, corresponding to $E_{c.m.}/V_B = 0.98$. The three different regions indicating $\Delta Z = 0, 1, 2$ transfer are labeled. Calculated energy-loss curves for different PLFs are shown by the dashed curves (see text). Bottom panel: $\Delta E_{gas}-E_{Si}$ spectrum for the scattering measurement of ^{12}C with a thick ^{181}Ta target during the same experiment at the indicated energy, giving an experimental ^{12}C energy-loss curve for the detector telescope, which is well reproduced by the calculated energy-loss curve for ^{12}C (see text).

and $1p1n$ stripping reactions (see Table I). However, ^{12}C and ^{14}C ions lose a different amount of energy ΔE_{gas} in the gas of the detector telescope. For measurements near the fusion barrier, the difference in energy loss for the ^{12}C and ^{14}C PLFs was calculated to be ~0.5 MeV. The dashed curves in Fig. 2 show the calculated energy losses for the carbon isotopes $^{12,13,14}C$, using the code STROP3, which uses stopping power values from Ref. [46]. The locus of the majority of the measured $\Delta Z = 2$ events in the top panel of the figure coincides with the energy-loss curve for ^{14}C. This suggests that the majority of $\Delta Z = 2$ events originate from the $2p$ transfer reaction leading to ^{14}C, with a secondary contribution from $2p1n$ and $\alpha(\equiv 2p2n)$-particle transfer. However, the unique identification of events with a particular transfer process depends critically on the accuracy of the energy-loss calculations, which in turn depend on the correct modeling of the detector and the accuracy of the stopping power tables used.

To determine the accuracy of the calculated energy-loss curves (as shown in Fig. 2), in the same experiment we used beams of $^{12,13}C$, scattered from a thick tantalum target to give experimental energy-loss curves for the detector telescope. These measurements were reproduced extremely well by the STROP3 calculations. This is illustrated by the comparison of the experimental energy losses for the elastically scattered ^{12}C particles with those calculated, shown in the bottom panel of Fig. 2.

Based on the energy-loss calculations, a new quantity, the *relative energy loss* ΔE_{rel}, was then defined. This corresponds to the difference between the measured energy loss of the $\Delta Z = 2$ PLFs and the calculated energy loss of ^{14}C. The ΔE_{rel} spectrum is essentially independent of differences in kinetic energy of the PLFs, thus presenting a useful tool for (i) identifying the dominant transfer processes and (ii) determining their corresponding absolute probabilities integrated over all final states in the residual nuclei. Figure 3 shows the ΔE_{rel} spectra for the measured elastically scattered ^{12}C and

TABLE I. Reaction ground-state Q values for selected transfer processes in the reaction ^{16}O + ^{208}Pb. Processes with a plus sign correspond to pickup; a minus sign indicates stripping. Predominant processes as determined by our measurements and previous work [34,45] are highlighted in bold.

	Reaction	Process	Q_{gs} (MeV)
$\Delta Z = 0$	^{208}Pb(^{16}O,^{17}O)^{207}Pb	**+1*n***	−3.225
	^{208}Pb(^{16}O,^{18}O)^{206}Pb	**+2*n***	−1.918
	^{208}Pb(^{16}O,^{15}O)^{209}Pb	$-1n$	−11.727
$\Delta Z = 1$	^{208}Pb(^{16}O,^{15}N)^{209}Bi	**−1*p***	−8.328
	^{208}Pb(^{16}O,^{14}N)^{210}Bi	$-1p-1n$	−14.557
	^{208}Pb(^{16}O,^{16}N)^{208}Bi	$-1p+1n$	−13.299
$\Delta Z = 2$	^{208}Pb(^{16}O,^{14}C)^{210}Po	**−2*p***	−13.553
	^{208}Pb(^{16}O,^{13}C)^{211}Po	$-2p-1n$	−17.178
	^{208}Pb(^{16}O,^{12}C)^{212}Po	**−2*p* − 2*n***	−16.116
	^{208}Pb(^{16}O,^{15}C)^{209}Po	$-2p+1n$	−19.993
	^{208}Pb(^{16}O,^{16}C)^{208}Po	$-2p+2n$	−22.710

^{13}C beam particles, shaded green and red, respectively. The centroids coincide with the calculated energy losses for ^{12}C and ^{13}C (indicated by the vertical lines), therefore confirming the accuracy of the energy-loss calculations as shown by the dashed curves in Fig. 2. The relative-energy-loss spectrum for the $\Delta Z = 2$ transfer events measured in the ^{16}O induced reaction is shown by the thick histogram in Fig. 3 for an incident ^{16}O beam energy corresponding to $E_{c.m.}/V_B = 0.98$. The majority of these $\Delta Z = 2$ events lie at ΔE_{rel} values *above* the centroids of the ^{12}C and ^{13}C events. This identifies the

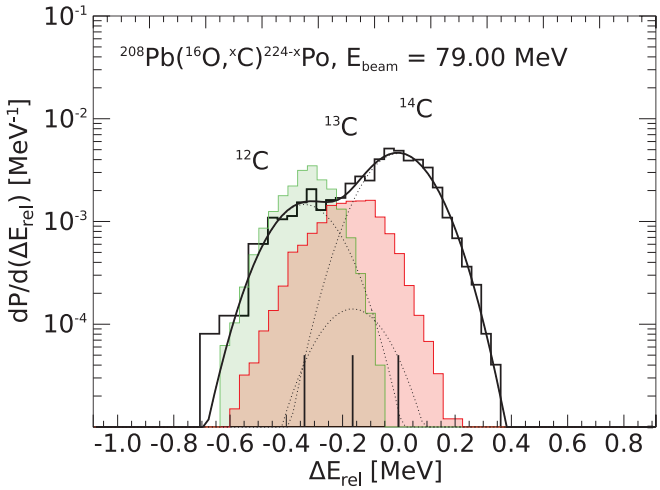

FIG. 3. (Color online) Relative energy loss ΔE_{rel} of the $\Delta Z = 2$ transfer events (thick black histogram) relative to the calculated energy loss of ^{14}C (see text) for an incident oxygen beam on a lead target at the indicated energy. Histograms of the relative energy losses for the elastic scattering measurements using beams of ^{12}C and ^{13}C made during the same experiment are shown by the green and red shaded areas, respectively. The Gaussian fits (dotted curves) correspond to $2p$, $2p1n$, and α-particle transfer leading to ^{14}C, ^{13}C, and ^{12}C ejectiles; the envelope of the fits is shown by the solid (black) curve. Calculated relative energy losses for the three indicated transfer reactions are indicated by the vertical lines.

majority of these events with ^{14}C ejectiles, produced following the $2p$ stripping reaction ^{208}Pb(^{16}O,^{14}C)^{210}Po.

B. Transfer probabilities

The experimental transfer probability for a process i is given by

$$P_i = \mathcal{N}\frac{N_i}{N_{\text{Ruth}}},$$

where N_i are the number of transfer events for process i, N_{Ruth} is the number of Rutherford scattering events, and $\mathcal{N}$ is the absolute normalization constant. N_{Ruth} is given by the total number of counts in the two forward angle detectors for each energy. Overall normalization $\mathcal{N}$ of the probabilities was achieved following the procedure detailed in Ref. [48].

1. *Element separation*

For measurements with the $\Delta E_{gas}-E_{Si}$ detector telescope, transfer events for processes with different ΔZ were extracted by gating on the particular region of interest in the $\Delta E_{gas}-E_{Si}$ spectra. For measurements where only a Si detector was used, transfer probabilities for processes leading to PLFs with different Z could still be extracted due to the well-separated reaction Q values for the predominant transfer processes (as determined by our measurements and previous work) in the reaction ^{16}O + ^{208}Pb (see Table I). The reliability of this method is demonstrated in the bottom three panels of Fig. 1, where individual energy spectra of events corresponding to identified oxygen, nitrogen, and carbon particles are shown. TKEL values were converted to excitation energies (corresponding to excited states in either the projectile-like or target-like fragment), by assuming elastic scattering for the oxygen, $1p$ stripping for the nitrogen, and $2p$ stripping for the carbon PLFs. It is clear from the individual energy spectra in the figure that, while excitation energies are as high as ∼13 MeV, the overlap in TKEL of different PLFs is small. This illustrates that events in different energy intervals in the TKEL energy spectra correspond to transfer processes with different ΔZ values. Thus (for measurements without the gas detector) transfer probabilities were extracted by integrating the number of counts in the TKEL spectra in a fixed energy interval.

Probabilities for the $\Delta Z = 1$ ($1p$ stripping) and $\Delta Z = 2$ transfer events are shown in Fig. 4 by the filled square and diamond symbols, respectively. The transfer probabilities are plotted as a function of the distance of closest approach, r_{min}, assuming a trajectory in a Coulomb plus nuclear potential. A Woods-Saxon parametrization of the nuclear potential was used:

$$V_N(r) = -\frac{V_0}{1+\exp\frac{r-R_0}{a_0}}, \quad (1)$$

where the parameters $V_0 = 80.0$ MeV, $r_0 = 1.191$ fm, and $a_0 = 0.671$ fm were determined from an analysis of the the total quasi-elastic scattering and the ^{208}Pb(3^-) excitation function within a coupled-channels framework as described

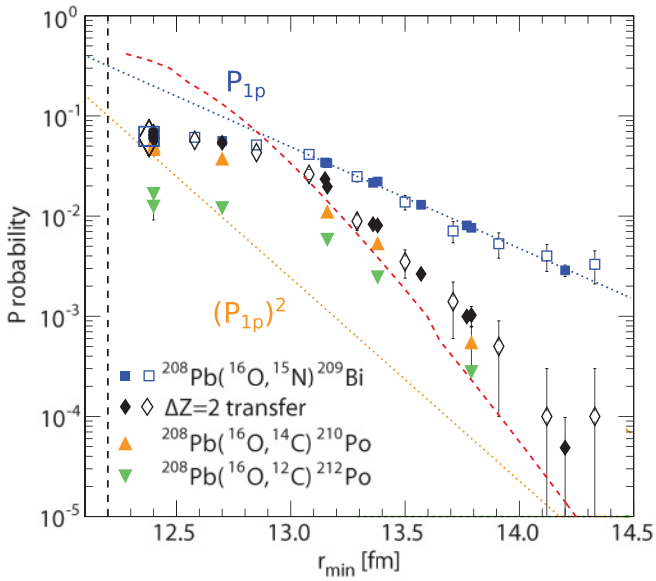

FIG. 4. (Color online) Measured transfer probabilities for the indicated transfer processes as a function of the distance of closest approach $r_{\rm min}$ assuming a trajectory in a Coulomb plus nuclear potential (see text). Filled symbols indicate results from this work. The large open square and diamond symbols at $r_{\rm min} \sim 12.4$ fm are the measurements for N (blue) and C PLFs (black) from Videbaek *et al.* [34]. The smaller open square and diamond symbols are unpublished measurements for N (blue) and C PLFs (black) from Timmers [47]. The asymptotic behaviors for the $1p$ transfer probability P_{1p} and purely sequential $2p$ transfer $P_{2p} = (P_{1p})^2$ are shown by the dotted lines (see text). The red dashed curve shows the fusion barrier penetrability (sub-barrier fusion probability) as calculated with the coupled-channels code CCFULL. The vertical dashed line indicates the average barrier radius r_B, corresponding to the experimental average fusion barrier energy $V_B = 74.5$ MeV [44].

in Refs. [15,48]. At energies well below the fusion barrier, $r_{\rm min}$ approaches the minimum distance under the assumption of a pure Coulomb trajectory [49] given by

$$r_{\rm min} \xrightarrow[E_{\rm c.m.} \ll V_B]{} r_{\rm min}^{\rm Coul} = \frac{Z_p Z_t e^2}{4\pi\epsilon_0} \frac{1}{2E_{\rm c.m.}} \left(1 + \mathrm{cosec}\,\frac{\theta_{\rm c.m.}}{2}\right),$$

where Z_p and Z_t are the atomic numbers of projectile and target nucleus, and $E_{\rm c.m.}$ and $\theta_{\rm c.m.}$ are the energy and scattering angle in the center-of-mass frame, respectively. As the energy increases $r_{\rm min}$ becomes smaller than $r_{\rm min}^{\rm Coul}$ due to the attractive nuclear potential.

The absolute probabilities agree very well with earlier unpublished measurements made at the Australian National University from Ref. [47], which are shown by the open square and diamond symbols for the N and C PLFs, respectively. Measurements also exist [34] for N and C PLFs at an energy around the fusion barrier (corresponding to $r_{\rm min} \sim 12.1$ fm). These are shown in Fig. 4 by the large open square and diamond symbols, respectively, which are also in excellent agreement. Since neither measurement allowed a separation in mass of the PLFs, as discussed in the introduction, it was commonly assumed that α-particle transfer was the dominant $\Delta Z = 2$ transfer process [28–31]. The flattening of the radial dependence seen in all measurements at energies (radial separations) close to the barrier can be associated with the absorption of flux due to sub-barrier fusion. A coupled-channels calculation of the probability for tunneling (penetrability) using the code CCFULL [50] is shown by the dashed curve in Fig. 4. Parameters for the real and imaginary potentials as well as coupling potentials were taken from Ref. [48].

2. *Isotope separation*

Contributions to the total $\Delta Z = 2$ transfer probability from $2p$, $2p1n$, and α-particle transfer were extracted by fitting a three-Gaussian distribution to the $\Delta E_{\rm rel}$ spectrum (see Fig. 3). The width of each individual Gaussian is fixed to the value of the width of the Gaussian-shaped elastically scattered ^{12}C distribution (green histogram in Fig. 3), and the relative energy losses among the three C isotopes are fixed to the values of the calculated energy losses for these particles. In Fig. 3 the envelope of the three-Gaussian fit is shown by the black solid curve, and the individual Gaussian components by the black dotted curves. Absolute probabilities for each $\Delta Z = 2$ transfer process were then obtained by evaluating the integral of the individual Gaussian functions of the three-Gaussian distribution and normalizing the sum of the three transfer probability components to the measured total $\Delta Z = 2$ transfer probability.

Extracted probabilities for the two transfer reactions ^{208}Pb(^{16}O,^{14}C)^{210}Po and ^{208}Pb(^{16}O,^{12}C)^{212}Po are shown in Fig. 4 by the orange upright and green inverted triangles, respectively. Transfer probabilities for the $2p1n$ stripping process ^{208}Pb(^{16}O,^{13}C)^{211}Po are not shown since they are $\sim$10 times smaller than those for α-particle transfer (see Fig. 3). At sub-barrier energies, $2p$ transfer (orange triangles in Fig. 4) is the dominant process. α-particle transfer probabilities (green triangles) are smaller by a factor of $\sim 2-4$ compared to those of $2p$ transfer. The difference in probabilities between $2p$ and α-particle transfer increases with increasing beam energy and is largest at $E_{\rm c.m.}/V_B \sim 1.0$ ($P_{2p} \sim 4 \times 10^{-2}$, $P_\alpha \sim 1 \times 10^{-2}$). It is interesting to note that absolute probabilities for $1p$, $2p$, and α-particle transfer at energies corresponding to $0.95 \leqslant E_{\rm c.m.}/V_B \leqslant 1.00$ ($13.3 \leqslant r_{\rm min} \leqslant 12.4$ fm) are comparable to the probability for populating the first excited state in ^{208}Pb (the octupole vibrational state at excitation energy 2.615 MeV. This shows that a consistent description of both inelastic *and* transfer channels within coupled-channels models may already be important at energies well below the fusion barrier in this reaction.

C. Transfer mechanisms

Insights into the transfer mechanisms and the significance of pairing correlations may be obtained by investigating the radial dependence of the transfer form factor at large separation distances (i.e., for $r_{\rm min} > r_B$, where r_B is the fusion barrier radius corresponding to the average fusion barrier energy V_B). The asymptotic behavior of the probability for transfer process i integrated over all final states of the residual nuclei is given

by [18,23]

$$P_i \propto \exp(-2\kappa_i r_{\min}), \tag{2}$$

where κ_i is the slope parameter for transfer process i. In the case of neutron transfer, the slope parameter κ_i can be simply related to the binding energy of the transferred neutron. For charged particle transfer this relation is more complex; however, final-state integrated transfer probabilities for charged particle transfer may be treated within the same semiclassical framework giving rise to Eq. (2) (see Ref. [11]).

The asymptotic behavior for $1p$ transfer (P_{1p}) was obtained by fitting the experimental data in Fig. 4 with a function of the form given by Eq. (2) in the region $13.0 \leqslant r_{\min} \leqslant 14.5$ fm and is shown by the dotted blue line in Fig. 4. In the absence of pairing correlations between the transferred nucleons, the probability for sequential two-nucleon transfer can be estimated by the square of the single-nucleon transfer probabilities. The resulting transfer probabilities for sequential uncorrelated $2p$ transfer $(P_{1p})^2$ are shown by the dotted orange line in Fig. 4. A significant enhancement of the observed $2p$ transfer probability is observed, by about one order of magnitude, indicating that $2p$ transfer does not follow the (simplistic) semiclassical picture of sequential transfer.

1. Comparison with TDHF calculations

Let us now compare the experimental data with purely sequential transfer predictions extracted from TDHF calculations of the two colliding nuclei. Both nuclei are initially in their Hartree-Fock ground state. The TDHF3D code developed by Bonche *et al.* [51] was used with a full Skyrme-type interaction [52]. The TDHF model is based on the independent particle picture and thus implicitly includes all single-particle excitations in the projectile- and target-like nuclei. The calculation of probabilities for transfer processes with different ΔZ is possible using a particle number projection technique on the projectile-like fragment [35]. These calculated TDHF transfer probabilities are automatically integrated over all final states in the residual nuclei. Since two-particle correlations are not included in the TDHF model, any deviation of the experimental data from the TDHF predictions could be attributed to an effect of such correlations. Thus a comparison of calculated and experimental probabilities for $\Delta Z = 1$ and $\Delta Z = 2$ transfer allows an estimate of the contribution from correlated nucleon transfer to the observed $\Delta Z = 2$ transfer excitation function.

Results for the $\Delta Z = 1$ ($1p$ stripping) and $\Delta Z = 2$ ($2p$ and α-particle stripping) transfer probabilities are presented in Fig. 5. The energy dependence of the TDHF calculations agree very well with $\Delta Z = 1$ transfer probabilities, albeit that the TDHF calculations over-predict the $\Delta Z = 1$ transfer excitation function by a factor of $\sim$2. In contrast, for $2p$ and α-particle transfer, the measured $\Delta Z = 2$ probabilities are much higher than the TDHF calculations ($P^{\text{measured}}_{\Delta Z=2} \sim 10 \times P^{\text{TDHF}}_{\Delta Z=2}$ at an energy corresponding to $E_{\text{c.m.}}/V_B \sim 0.96$). Both the overestimation of the $\Delta Z = 1$ and the underestimation of the $\Delta Z = 2$ channels in the TDHF calculations suggest that there is a strong pairing correlation between the two transferred protons. It is interesting to note that the square of the TDHF

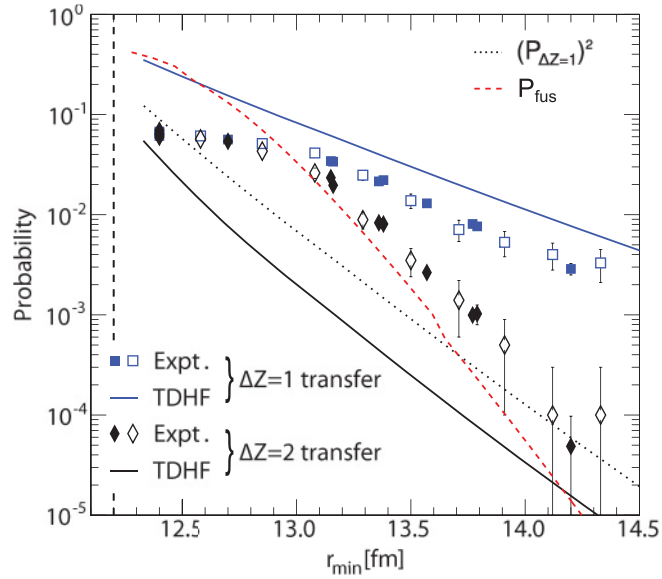

FIG. 5. (Color online) TDHF calculations of the $\Delta Z = 1$ ($1p$ stripping) and $\Delta Z = 2$ ($2p$ and α-particle stripping) transfer excitation functions as a function of the distance of closest approach $r_{\min}$, shown by the full curves. Experimental data are the same as in Fig. 4. The vertical dashed line indicates the average barrier radius. The dotted curve shows the square of the TDHF $\Delta Z = 1$ transfer probabilities. The red dashed curve shows the fusion barrier penetrability (sub-barrier fusion probability) as calculated with the coupled-channels code CCFULL.

$\Delta Z = 1$ transfer probabilities $(P^{\text{TDHF}}_{\Delta Z=1})^2$ (shown by the dotted curve in Fig. 5) does not reproduce the TDHF probabilities for $\Delta Z = 2$ transfer $P^{\text{TDHF}}_{\Delta Z=2}$. This can be understood by the fact that the probability for transferring a proton from the projectile-like to the target-like nucleus may change significantly after the transfer of the first proton. The change in the $1p$ transfer probability depends on the change in the Q value, kinematics, and different nuclear structure of the interacting nuclei. The divergence of the TDHF calculations from the measured transfer probabilities at energies close to the barrier occurs because sub-barrier fusion (which is not present in the TDHF model) becomes non-negligible at energies closer to the fusion barrier. The CCFULL fusion barrier penetrability is again shown by the dashed curve in Fig. 5. It is important to note that the fusion barrier predicted by the TDHF model [35], $V_B^{\text{TDHF}} = 74.44 \pm 0.005$ MeV, is almost identical to the experimental average barrier of $V_B = 74.5$ MeV [44].

Concluding the discussion of transfer probabilities, we have measured the $\Delta Z = 1$ ($1p$ stripping) and $\Delta Z = 2$ ($2p$ and α-particle stripping) transfer probabilities for the reaction ^{16}O + ^{208}Pb down to energies well below the fusion barrier. It was found that $2p$ transfer is the dominant $\Delta Z = 2$ transfer process, at least down to energies corresponding to $E_{\text{c.m.}}/V_B \sim 0.9$. The $2p$ transfer probability reaches a maximum of $\sim$10% at a beam energy around the fusion barrier energy. It is enhanced by a factor of $\sim$10 at sub-barrier energies compared to predictions based on the independent particle pictures simulated with the fully microscopic time-dependent

Hartree-Fock model. While single-particle excitations in the projectile- and target-like nuclei are implicitly included in the TDHF calculations, two-nucleon correlations are beyond the TDHF model space. Thus the observed strong enhancement of the $\Delta Z = 2$ transfer probabilities on one side, and the hindrance of the $\Delta Z = 1$ transfer probabilities on the other side, indicate a strong pairing correlation between the two transferred protons. While the enhancement of the $2p$ transfer probabilities is consistent with measurements for ^{16}O-induced reactions on closed neutron-shell and open proton-shell targets at energies near and above the fusion barrier [43], the significance of $2p$ transfer already at energies well below the fusion barrier demonstrates that pairing correlations in ^{16}O play an important role in reaction mechanisms.

III. EXCITATION ENERGIES

Excitation energy spectra for PLFs resulting from transfer with $\Delta Z = 0$, 1, and 2 were derived as explained in Sec. II and are shown in Fig. 1 for a beam energy corresponding to $E_{\mathrm{c.m.}}/V_B = 0.98$. For $\Delta Z = 0$ and $\Delta Z = 1$ most of the intensity lies in discrete peaks that can be identified with one or more excited states in the two residual nuclei. In contrast, for $\Delta Z = 2$ the situation is different. Excitation energies extend to $\sim$13 MeV, and the spectrum shows a continuum-like structure instead of clearly identifiable discrete peaks. This structure is visible for all measurements at sub-barrier energies, the maximum of which moves toward larger excitation energies for higher beam energies. This shift occurs at a faster rate than is predicted from optimum Q-value considerations. The $\Delta Z = 2$ excitation energy spectra show that correlated $2p$ transfer leads to the population of highly excited states in the residual nuclei.

In collisions at above-barrier energies the population of highly excited states via DICs is widely understood as the dissipation of kinetic energy into the internal nucleonic degrees of freedom of the residual nuclei. The strong population of highly excited states at sub-barrier energies therefore poses the question of whether a treatment of the processes leading to these highly excited states within the coupled channels framework will lead to a correct description of sub-barrier collisions, or if instead the dissipation of energy to nucleonic degrees of freedom already at sub-barrier energies needs to be taken into account.

IV. CONCLUSION

Measurements presented in this work show that in the reaction $^{16}O + ^{208}Pb$ correlated $2p$ transfer occurs with a significant probability. The probability is comparable to that for $1p$ transfer and for populating the first excited state in ^{208}Pb. Following $2p$ transfer, the residual nuclei are left in highly excited states. The measurements and results presented are a step toward a full and consistent understanding of transfer processes in themselves and their relationship with other reaction processes such as deep inelastic collisions and fusion. It has been a challenge for many decades to simultaneously reproduce all observables related to individual reaction processes (elastic scattering, transfer, fusion, etc.) for the $^{16}O + ^{208}Pb$ reaction at sub- and near-barrier energies. It has been suggested that the observed hindrance of fusion at deep sub-barrier energies [4] may be related to irreversible reaction processes, suppressing the tunneling probability. Recent results based on fully microscopic reaction model calculations suggest that a realistic description of particle transfer at energies below the barrier involves the inclusion of reversible fluctuations of the number of nucleons in each nucleus, particle correlations, and irreversible dissipation [53–55]. However, a microscopic theory including also sub-barrier fusion is still unavailable, and only coupled-channels approaches are currently able to describe all reaction channels simultaneously around the fusion barrier. Thus in a first step we believe that results presented in this work will provide crucial input parameters for developing an improved phenomenological model to allow the simultaneous description of all reaction processes at energies well below and above the fusion barrier energy.

ACKNOWLEDGMENTS

M.E. would like to thank W. von Oertzen for his insightful remarks and comments after reading this paper. The authors acknowledge the financial support of Australian Research Council Discovery Grants No. DP0879679 and No. DP110102879.

[1] M. Dasgupta, D. J. Hinde, N. Rowley, and A. M. Stefanini, Annu. Rev. Nucl. Part. Sci. **48**, 401 (1998).
[2] C. L. Jiang *et al.*, Phys. Rev. Lett. **89**, 052701 (2002).
[3] C. L. Jiang *et al.*, Phys. Rev. C **71**, 044613 (2005).
[4] M. Dasgupta, D. J. Hinde, A. Diaz-Torres, B. Bouriquet, C. I. Low, G. J. Milburn, and J. O. Newton, Phys. Rev. Lett. **99**, 192701 (2007).
[5] H. Esbensen and S. Misicu, Phys. Rev. C **76**, 054609 (2007).
[6] T. Ichikawa, K. Hagino, and A. Iwamoto, Phys. Rev. Lett. **103**, 202701 (2009).
[7] K. Hagino, S. Yusa, and N. Rowley, Nucl. Phys. A **834**, 135c (2010).
[8] L. Corradi, Nucl. Phys. A **834**, 129c (2010), the 10th International Conference on Nucleus-Nucleus Collisions (NN2009).
[9] M. Evers, Ph.D. thesis, Australian National University, 2010.
[10] J. O. Newton, R. D. Butt, M. Dasgupta, D. J. Hinde, I. I. Gontchar, C. R. Morton, and K. Hagino, Phys. Rev. C **70**, 024605 (2004).
[11] K. E. Rehm, Annu. Rev. Nucl. Part. Sci. **41**, 429 (1991).
[12] H. Timmers, J. R. Leigh, M. Dasgupta, D. J. Hinde, R. C. Lemmon, J. C. Mein, C. R. Morton, J. O. Newton, and N. Rowley, Nucl. Phys. A **584**, 190 (1995).
[13] K. Hagino, T. Takehi, A. B. Balantekin, and N. Takigawa, Phys. Rev. C **71**, 044612 (2005).
[14] L. R. Gasques, M. Evers, D. J. Hinde, M. Dasgupta, P. R. S. Gomes, R. M. Anjos, M. L. Brown, M. D. Rodriguez, R. G. Thomas, and K. Hagino, Phys. Rev. C **76**, 024612 (2007).

[15] M. Evers, M. Dasgupta, D. J. Hinde, L. R. Gasques, M. L. Brown, R. Rafiei, and R. G. Thomas, Phys. Rev. C **78**, 034614 (2008).
[16] E. Piasecki *et al.*, Phys. Rev. C **80**, 054613 (2009).
[17] S. Yusa, K. Hagino, and N. Rowley, Phys. Rev. C (to be published).
[18] W. von Oertzen and A. Vitturi, Rep. Prog. Phys. **64**, 1247 (2001).
[19] E. E. B. Campbell and F. Rohmund, Rep. Prog. Phys. **63**, 1061 (2000).
[20] R. A. Broglia, C. H. Dasso, S. Landowne, B. S. Nilsson, and A. Winther, Phys. Lett. B **73**, 401 (1978).
[21] I. Chiodi *et al.*, Lett. Nuovo Cimento **33**, 159 (1982).
[22] M. C. Mermaz and M. Girod, Phys. Rev. C **53**, 1819 (1996).
[23] L. Corradi, G. Pollarolo, and S. Szilner, J. Phys. G **36**, 113101 (2009).
[24] L. Corradi *et al.*, Phys. Rev. C **84**, 034603 (2011).
[25] V. I. Goldanskii, Phys. Lett. **14**, 233 (1965); K. Dietrich, Ann. Phys. (NY) **66**, 480 (1971).
[26] C. H. Dasso and G. Pollarolo, Phys. Rev. C **39**, 2073 (1989).
[27] K. E. Rehm, A. M. van den Berg, J. J. Kolata, D. G. Kovar, W. Kutschera, G. Rosner, G. S. F. Stephans, and J. L. Yntema, Phys. Rev. C **37**, 2629 (1988).
[28] R. M. DeVries, D. Shapira, W. G. Davies, G. C. Ball, J. S. Forster, and W. McLatchie, Phys. Rev. Lett. **35**, 835 (1975).
[29] H. Hasan and C. S. Warke, Nucl. Phys. A **318**, 523 (1979).
[30] I. J. Thompson, M. A. Nagarajan, J. S. Lilley, and M. J. Smithson, Nucl. Phys. A **505**, 84 (1989).
[31] T. Tamura, T. Udagawa, and M. C. Mermaz, Phys. Rep. **65**, 345 (1980).
[32] F. D. Becchetti, D. G. Kovar, B. G. Harvey, D. L. Hendrie, H. Homeyer, J. Mahoney, W. von Oertzen, and N. K. Glendenning, Phys. Rev. C **9**, 1543 (1974).
[33] U. Götz, M. Ichimura, R. A. Broglia, and A. Winther, Phys. Rep. **16**, 115 (1975).
[34] F. Videbaek, R. B. Goldstein, L. Grodzins, S. G. Steadman, T. A. Belote, and J. D. Garrett, Phys. Rev. C **15**, 954 (1977).
[35] C. Simenel, Phys. Rev. Lett. **105**, 192701 (2010).
[36] C. J. G. Onderwater *et al.*, Phys. Rev. Lett. **78**, 4893 (1997).
[37] W. H. A. Hesselink, R. Starink, W. H. A. Hesselink, D. L. Groep, E. Jans, and R. Starink, Prog. Part. Nucl. Phys. **44**, 89 (2000).
[38] W. H. Dickhoff, J. Phys. G **37**, 1 (2010).
[39] Y. Funaki, T. Yamada, H. Horiuchi, G. Röpke, P. Schuck, and A. Tohsaki, Phys. Rev. Lett. **101**, 082502 (2008).
[40] M. N. A. Abdullah, S. Hossain, M. S. I. Sarker, S. K. Das, A. S. B. Tariq, M. A. Uddin, A. K. Basak, S. Ali, H. M. S. Gupta, and F. B. Malik, Eur. Phys. J. A **18**, 65 (2003).
[41] C. Wheldon *et al.*, Phys. Rev. C **83**, 064324 (2011).
[42] F. D. Becchetti, B. G. Harvey, D. Kovar, J. Mohoney, C. Maguire, and D. K. Scott, Phys. Rev. C **12**, 894 (1975).
[43] W. von Oertzen, H. G. Bohlen, and B. Gebauer, Nucl. Phys. A **207**, 91 (1973).
[44] C. R. Morton, A. C. Berriman, M. Dasgupta, D. J. Hinde, J. O. Newton, K. Hagino, and I. J. Thompson, Phys. Rev. C **60**, 044608 (1999).
[45] S. C. Pieper *et al.*, Phys. Rev. C **18**, 180 (1978).
[46] J. F. Ziegler, J. P. Biersack, and U. Littmark, *The Stopping and Range of Ions in Solids*, The Stopping and Ranges of Ions in Matter, Vol. 1 (Pergamon, New York, 1985).
[47] H. Timmers, Ph.D. thesis, Australian National University, 1996, [http://www.pems.adfa.edu.au/∼s9471553/level1/pdffiles/thesisabstract.html].
[48] M. Evers, D. J. Hinde, M. Dasgupta, D. H. Luong, R. Rafiei, and R. du Rietz, Phys. Rev. C **81**, 014602 (2010).
[49] R. A. Broglia and A. Winther, *Heavy Ion Reactions (Lecture Notes), Volume 1: Elastic and Inelastic Reactions* (Benjamin/Cummings, New York, 1981).
[50] K. Hagino, N. Rowley, and A. T. Kruppa, Comput. Phys. Commun. **123**, 143 (1999).
[51] P. Bonche, H. Flocard, and P. Heenen, Nucl. Phys. A **467**, 115 (1987).
[52] K.-H. Kim, T. Otsuka, and P. Bonche, J. Phys. G **23**, 1267 (1997).
[53] M. Assié and D. Lacroix, Phys. Rev. Lett. **102**, 202501 (2009).
[54] C. Simenel, Phys. Rev. Lett. **106**, 112502 (2011).
[55] K. Washiyama, S. Ayik, and D. Lacroix, Phys. Rev. C **80**, 031602 (2009).